APL Materials

High-order harmonic generation from hybrid organic–inorganic perovskite thin films

Cite as: APL Mater. **7**, 041107 (2019); https://doi.org/10.1063/1.5090935
Submitted: 31 January 2019 . Accepted: 21 March 2019 . Published Online: 05 April 2019

Hideki Hirori, Peiyu Xia, Yasushi Shinohara, Tomohito Otobe, Yasuyuki Sanari, Hirokazu Tahara, Nobuhisa Ishii, Jiro Itatani, Kenichi L. Ishikawa, Tomoko Aharen, Masashi Ozaki, Atsushi Wakamiya, and Yoshihiko Kanemitsu

High-order harmonic generation from hybrid organic–inorganic perovskite thin films

Cite as: APL Mater. 7, 041107 (2019); doi: 10.1063/1.5090935
Submitted: 31 January 2019 • Accepted: 21 March 2019 •
Published Online: 5 April 2019

View Online Export Citation CrossMark

Hideki Hirori,[1] Peiyu Xia,[2] Yasushi Shinohara,[3,4] Tomohito Otobe,[5] Yasuyuki Sanari,[1] Hirokazu Tahara,[1] Nobuhisa Ishii,[2] Jiro Itatani,[2] Kenichi L. Ishikawa,[3,4,6] Tomoko Aharen,[1] Masashi Ozaki,[1] Atsushi Wakamiya,[1] and Yoshihiko Kanemitsu[1,a)]

AFFILIATIONS

[1]Institute for Chemical Research, Kyoto University, Uji, Kyoto 611-0011, Japan
[2]Institute for Solid State Physics, the University of Tokyo, Kashiwa, Chiba 277-8581, Japan
[3]Photon Science Center, Graduate School of Engineering, the University of Tokyo, Bunkyo-ku, Tokyo 113-8656, Japan
[4]Department of Nuclear Engineering and Management, Graduate School of Engineering, the University of Tokyo, Bunkyo-ku, Tokyo 113-8656, Japan
[5]Kansai Photon Science Institute, National Institutes for Quantum and Radiological Science and Technology, Kizugawa, Kyoto 619-0615, Japan
[6]Research Institute for Photon Science and Laser Technology, the University of Tokyo, Bunkyo-ku, Tokyo 113-0033 Japan

[a)]**Author to whom correspondence should be addressed:** kanemitu@scl.kyoto-u.ac.jp

ABSTRACT

The generation of high-order harmonics from hybrid organic–inorganic perovskites (HOIPs) is demonstrated by the excitation with a strong mid-infrared laser pulse. We prepare three types of HOIP polycrystalline thin film samples by solution processes ($MAPbX_3$; MA = $CH_3NH_3^+$; X = I, Br, Cl). The high-order harmonics from the sample ($MAPbBr_3$) are more than tenfold stronger than those from the well-studied GaSe crystal despite their comparable bandgap energies, implying that the stronger band-to-band transition of the HOIPs causes the higher yields.

In recent years, the materials system of the hybrid organic–inorganic perovskites (HOIPs) has attracted attention as optoelectronic semiconductors that can be applied in high-performance photovoltaic devices.[1,2] This class of materials exhibits excellent electrical and optical properties such as high carrier mobility, tunable optoelectronic properties, and high fluorescence yields. Together with these excellent properties, the fact that HOIPs are high-quality materials that can be manufactured with low-temperature solution processes has made them promising candidates for optoelectronic devices such as lasers, light emitting diodes (LEDs), photodetectors, and photodiodes.[3–6] Besides the applications noted above, the interest in research regarding the application to nonlinear optical elements has also been increasing, and the saturable absorption effect required for the development of mode-locked fiber lasers and also the two-photon-absorption process required for two-photon pumped lasing have been demonstrated for bulk and nanostructured materials.[7–10]

Recently, the high-order harmonic generation (HHG) is being intensively investigated in the area of extreme nonlinear optical interactions between solids and intense terahertz (THz) or mid-infrared (MIR) light pulses.[11–13] This phenomenon attracts attention from the viewpoint of application in development of bright light sources ranging from visible to extreme ultraviolet (EUV or XUV) optical field and attosecond photonics.[11–18] It shows also promise for the development of all-optical ultrafast electronics and band structure reconstruction methodologies. Since the HOIPs can be made by a solution process, the realization of HHG with these samples may allow the convenient fabrication of large-area emitters for high power HHG sources and also of the cavity structures for compact ones.

In this work, we illuminate three types of polycrystalline HOIP [$MAPbX_3$; MA (methylammonium) = $CH_3NH_3^+$ and X being either I, Br, or Cl] thin film samples with a thickness of 200 nm and demonstrate an emission of high-order harmonics with a strong MIR laser

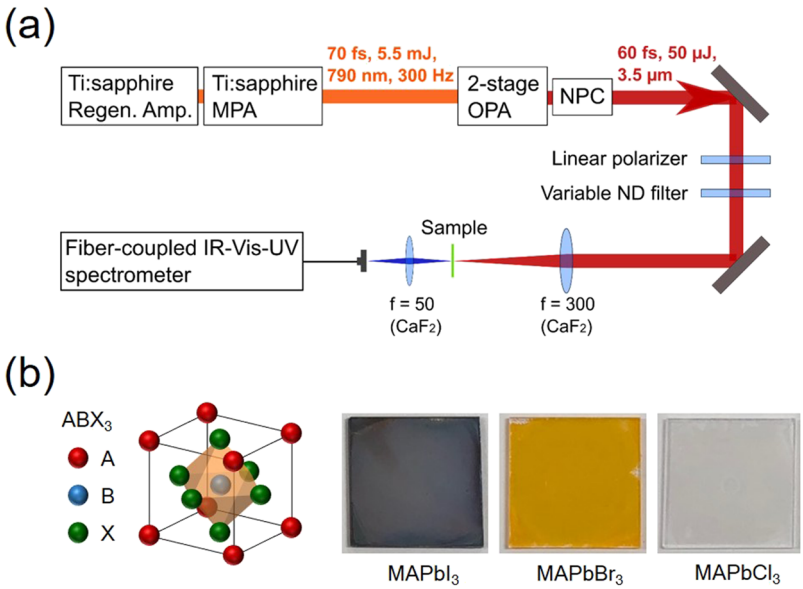

FIG. 1. (a) Experimental setup for HHG measurement. Regen. Amp., regenerative amplifier; MPA, multipass amplifier; OPA, optical parametric amplifier; and NPC, nonlinear pulse compression. (b) The schematics of a perovskite ABX_3 crystal structure where A = $CH_3NH_3^+$ (MA), B = Pb, and X = I, Br, or Cl and photographs of polycrystalline HOIP thin films (thickness 0.2 μm) on the quartz substrate (1 × 25 × 25 mm^3).

pulse. The high-order harmonics from the sample ($MAPbBr_3$) are more than tenfold stronger than those from the well-studied GaSe crystal despite their comparable bandgap energies,[12,17] implying that the stronger band-to-band transition of the HOIPs causes the higher yields. Harmonics up to the 13th order (a photon energy of 4.6 eV) are clearly visible in the spectra from the $MAPbCl_3$ film. This indicates that $MAPbCl_3$ had a larger bandgap energy E_g than the other samples, and reabsorption of the propagating harmonic components was suppressed in it. A numerical simulation based on an *ab-initio* theoretical framework for $MAPbCl_3$ indicates that the valence band maximum (VBM) component has dominant contribution among the intraband contribution.

As shown in Fig. 1(a), the MIR laser pulses at 3.5 μm (0.35 eV) from a $KTiOAsO_4$ (KTA)-based optical parametric amplifier were used for the excitation of samples in the HHG measurement.[19] To achieve higher peak electric fields, the MIR pulses after OPA stages were compressed by spectral broadening in a germanium plate followed by dispersion compensation in sapphire and fused silica plates, which is abbreviated as NPC in Fig. 1. The pulse duration was measured to be 60 fs by second-harmonic generation frequency-resolved optical gating. These pulses were focused onto the polycrystalline HOIP thin film samples, and the propagation axis of the excitation light was normal to the sample surface. The maximum pulse energy focused at the sample position was 16 μJ with a spot size of 370 μm (diameter at 1/e^2) obtained via the knife-edge method. Regarding the linear polarized light, this corresponds to a maximum electric field amplitude of 19 MV/cm in the air and 13 MV/cm inside the samples. The harmonics generated in and transmitted through the sample were measured with a charge-coupled-device camera sensitive to the visible and ultraviolet regions and an InGaAs array detector sensitive to the near-infrared region.

Materials of the HOIP samples are in the perovskite structure (ABX_3; A is the organic cation, B is the metallic cation, and X is the halide anion) after crystallization from the organic halide and the metallic halide salts [see Fig. 1(b)]. Through replacement of both the cation and the anion, the bandgap energy E_g of the HOIPs is tunable over a wide range; the E_g of the samples employed in the experiment increased from 1.55 (I) to 2.3 eV (Br) and to 3.2 eV (Cl) by anion exchange. All film samples were synthesized using anti-solvent dripping method.[20] The perovskite precursor solutions for the $MAPbI_3$ and $MAPbBr_3$ thin films were prepared by dissolving equimolar MAI (1mmol) (or MABr, 1 mmol) and PbI_2 (1 mmol) (or $PbBr_2$, 1 mmol) in a DMF/DMSO (4:1, 1 ml in total) solvent mixture. The precursor solution for the $MAPbCl_3$ thin films was

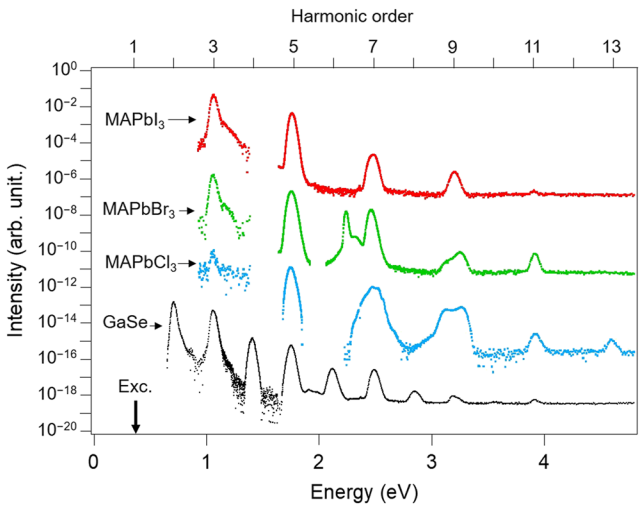

FIG. 2. HHG spectra from hybrid lead halide perovskites. HHG spectra of polycrystalline HOIP thin films ($MAPbX_3$; X = I, Br, Cl; thickness 0.2 μm) and a GaSe sample (thickness 1 μm; for reference) are shown. The fundamental field (mid-infrared excitation pulse) is centered at a photon energy of 0.35 eV, as indicated by the vertical arrow on the bottom axis. The data are offset for clarity.

prepared by dissolving equimolar MACl and $PbCl_2$ (0.5 mmol each) in a DMF/DMSO (1:1, 1 ml) solvent mixture. The solutions were dispensed on pre-cleaned quartz substrates and spun at 5000 rpm for 20 s, followed by annealing at 70 °C for 25 min to complete the thin film formation. During the spinning period, toluene was dripped onto the film surfaces to obtain mirror-like flat surfaces.

Figure 2 shows that the three types of film samples exhibit harmonics from the visible to the ultraviolet region. The spectra show only odd harmonics and a fluorescence with amplified spontaneous emission around 2.3 eV (Br);[21] the absence of even harmonics originates from the inversion symmetry of the perovskite crystal structure. Although the grain structures with size up to micrometer scales can be formed in the solution-based film samples, the much larger size of the laser spot (370 μm) would allow cancelation of the even components from the grain boundary. In the $MAPbCl_3$ sample, which has a larger bandgap energy E_g of 3.15 eV than the others, the reabsorption of the propagating harmonic components is suppressed,[22] and relatively higher components up to the 13th order (a photon energy of 4.6 eV) are obtained. As shown in Fig. 2, we also measured harmonics from a GaSe crystal with the same electric field strength to compare the HHG yields with the HOIP samples. The propagation axis of the MIR pulses was parallel to the *c*-axis of GaSe, which allows the generation of even-order harmonics due to the lack of inversion symmetry (the HHG spectra were measured without resolving the polarization of the harmonics).

Figure 3(a) compares the HHG intensities per unit thickness obtained from the HOIP thin films and from a GaSe crystal (see Fig. 2, thickness: 1 μm, $\alpha \sim 10^3$ cm^{-1}, E_g = 2.02 eV).[23] The high-order harmonics from the $MAPbBr_3$ sample are more than tenfold stronger than those from the GaSe crystal despite their comparable bandgap energies. Figure 3(b) shows the electric field dependences of the normalized intensity for several harmonic orders from $MAPbCl_3$. The behavior changes from perturbative in the weak excitation regime, where the intensity obeys a scaling law E^{2h} (h is an integer), to non-perturbative as the excitation becomes stronger. The organic molecule MA, which supports the perovskite structure, had a significant tolerance to laser illumination; there was no sample degradation that could have influence the HHG during the measurement.

To simulate the HHG spectra from $MAPbCl_3$, we calculated the temporal evolution of the current density $J(t)$ by using an *ab initio* quantum mechanical simulation.[24,25] This theoretical framework is essentially equivalent to that of the semiconductor Bloch equation (SBE).[26] Since MA cations are oriented randomly over macroscopic volume at room temperature and thus exhibit spherically symmetric behavior, in the calculation, we assumed a simplification of using a Cs cation (one of the best alternatives for simple calculations) instead of an MA cation. The band structure and the transition momentum were calculated using first-principles density functional theory (DFT). The electronic contributions of the MA and Cs cation appear several electron volts below the Fermi level because of the resulting weak electronic interaction between the cations and the inorganic part.[27,28] The MA and Cs play a role of maintaining the bone of the crystal to keep a certain distance among atoms and do not take part in optical activities due to electrons below the bandgap.

The HHG spectra can be obtained from the Fourier transform of the calculated total current density $J_{total}(t)$ (gray shaded area in Fig. 4) and can be decomposed into the intraband current $J_{intra}(\omega)$ due to acceleration of carrier wave packets in electronic bands and the interband current $J_{inter}(\omega)$ due to coherent emission from the polarization between dipole-coupled bands: $J_{total}(\omega) = J_{intra}(\omega) + J_{inter}(\omega)$. From Fig. 4, since $J_{intra}(t)$ contributes the most to $J_{total}(t)$, the intraband current term dominates the HHG in HOIPs. Furthermore, by decomposing the intraband current $J_{intra}(\omega)$, our analysis provides further insights into the HHG mechanism. Figure 4 shows that the high harmonic components due to $J_{intra}(\omega)$ closely follow those of the intraband current $J_{VBM}(\omega)$ originating from VBM (red dashed line), whose band is composed of a mixture of Cl 3*p* and Pb 6*s* orbitals. This feature differs from the usual assumption regarding the origin of HHG in the previous work, where the intraband current $J_{CB}(\omega)$ in the conduction band dominates $J_{intra}(\omega)$.

In general, the intraband current $j(t)$ is determined by the product of the carrier group velocity $v_g(k)$ and the carrier density $n(k, t)$ that is excited by the incident laser field, i.e., $j(t) = -ev_g(k)n(k, t)$. Here, e is the elementary charge and k is the wavenumber. This means that the generation efficiency of harmonics increases with the carrier density. The large joint density of states in HOIPs leads to an absorption coefficient ($\alpha \sim 10^5$ cm^{-1}) that is one-hundred times larger than that of GaSe. Thus, it can be inferred that the stronger

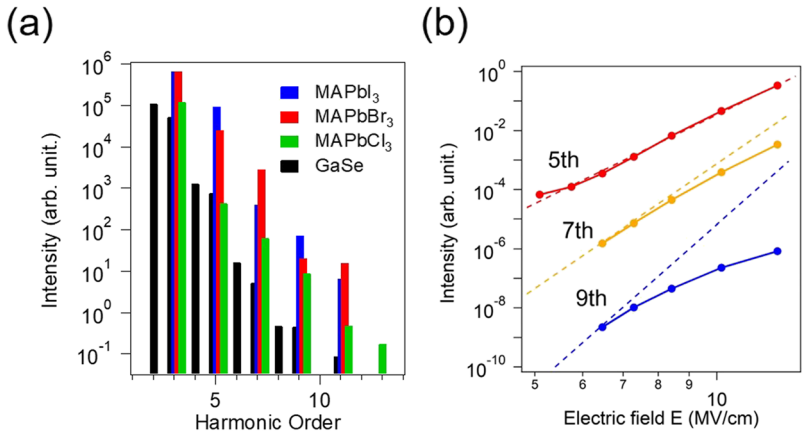

FIG. 3. (a) Comparison of the HHG intensities per unit thickness from the HOIPs film samples [$MAPbX_3$; X = I (blue bars), Br (red bars), Cl (green bars)] and GaSe crystal (black bars). (b) Normalized harmonic intensity for $MAPbCl_3$ film as a function of the peak electric field E inside the sample for harmonic orders h = 5, 7, and 9 (solid circles), respectively. The dashed lines are guides for the eye that are proportional to E^{2h}. The data sets are offset for clarity.

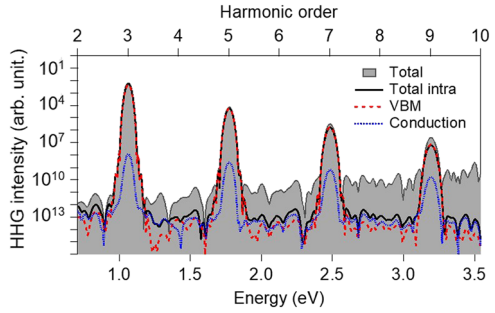

FIG. 4. Decomposition of the harmonic spectra calculated with a peak electric field E = 10 MV/cm. The gray filled region, black-solid line, red-dashed line, and blue-dotted line show total, intraband total, VBM, and conduction contributions, respectively.

nonlinear optical transitions may cause a stronger intraband current and a larger high-order harmonics intensity as shown in Fig. 3(b).

In conclusion, we illuminated HOIP thin films with a strong MIR laser pulse and demonstrated HHG that extends from the visible to the ultraviolet region. These HOIPs are potentially advantageous for the fabrication of large-area emitters for high power HHG sources and also of the cavity structures for compact ones because of their solution-processability. A numerical simulation indicates that the intraband acceleration of the holes in the valence band constitutes the dominant origin for the spectra of HHG. For the further understanding of the generation mechanism in the materials, it would be important to study the crystallographic orientation dependence of high-order harmonics yields for a single crystal.

This study was supported by CREST (Grant Nos. JPMJCR16N3 and JPMJCR15N1), PRESTO (Grant No. JPMJPR1427) grants, and the Center of Innovation Program from JST and KAKENHI (Grant Nos. 18H03682, 18K14145, 17K05089, 18K13481, and No. 16H03881) grants from JSPS and by the Exploratory Challenge on Post-K Computer and the Photon Frontier Network Program from MEXT. The computation in this work was done using the facilities of the Supercomputer Center (the Institute for Solid State Physics, the University of Tokyo) and also using the K computer provided by the RIKEN Advanced Institute for Computational Science through the HPCI System Research project (Project ID: hp170235).

REFERENCES

[1] A. Kojima, K. Teshima, Y. Shirai, and T. Miyasaka, J. Am. Chem. Soc. **131**, 6050–6051 (2009).
[2] M. Saliba, T. Matsui, K. Domanski, J.-Y. Seo, A. Ummadisingu, S. M. Zakeeruddin, J.-P. Correa-Baena, W. R. Tress, A. Abate, A. Hagfeldt, and M. Grätzel, Science **354**, 206–209 (2016).
[3] G. Xing, N. Mathews, S. S. Lim, N. Yantara, X. Liu, D. Sabba, M. Grätzel, S. Mhaisalkar, and T. C. Sum, Nat. Mater. **13**, 476–480 (2014).
[4] Z.-K. Tan, R. S. Moghaddam, M. L. Lai, P. Docampo, R. Higler, F. Deschler, M. Price, A. Sadhanala, L. M. Pazos, D. Credgington, F. Hanusch, T. Bein, H. J. Snaith, and R. H. Friend, Nat. Nanotechnol. **9**, 687–692 (2014).
[5] A. Sadhanala, S. Ahmad, B. Zhao, N. Giesbrecht, P. M. Pearce, F. Deschler, R. L. Z. Hoye, K. C. Gödel, T. Bein, P. Docampo, S. E. Dutton, M. F. L. De Volder, and R. H. Friend, Nano Lett. **15**, 6095–6101 (2015).
[6] Y. Kanemitsu and T. Handa, Jpn. J. Appl. Phys. **57**, 090101 (2018).
[7] Y. Yamada, T. Yamada, L. Q. Phuong, N. Maruyama, H. Nishimura, A. Wakamiya, Y. Murata, and Y. Kanemitsu, J. Am. Chem. Soc. **137**, 10456–10459 (2015).
[8] R. Zhang, J. Fan, X. Zhang, H. Yu, H. Zhang, Y. Mai, T. Xu, J. Wang, and H. J. Snaith, ACS Photon **3**, 371–377 (2016).
[9] P. Li, Y. Chen, T. Yang, Z. Wang, H. Lin, Y. Xu, L. Li, H. Mu, B. N. Shivananju, Y. Zhang, Q. Zhang, A. Pan, S. Li, D. Y. Tang, B. Jia, H. Zhang, and Q. Bao, ACS Appl. Mater. Interfaces **9**, 12759–12765 (2017).
[10] Y. Xu, Q. Chen, C. Zhang, R. Wang, H. Wu, X. Zhang, G. Xing, W. W. Yu, X. Wang, Y. Zhang, and M. Xiao, J. Am. Chem. Soc. **138**, 3761–3768 (2016).
[11] S. Ghimire, A. D. DiChiara, E. Sistrunk, P. Agostini, L. F. DiMauro, and D. A. Reis, Nat. Phys. **7**, 138–141 (2011).
[12] O. Schubert, M. Hohenleutner, F. Langer, B. Urbanek, C. Lange, U. Huttner, D. Golde, T. Meier, M. Kira, S. W. Koch, and R. Huber, Nat. Photon **8**, 119–123 (2014).
[13] D. Golde, T. Meier, and S. W. Koch, Phys. Rev. B **77**, 075330 (2008).
[14] T. T. Luu, M. Garg, S. Y. Kruchinin, A. Moulet, M. T. Hassan, and E. Goulielmakis, Nature **521**, 498–502 (2015).
[15] M. Garg, M. Zhan, T. T. Luu, H. Lakhotia, T. Klostermann, A. Guggenmos, and E. Goulielmakis, Nature **538**, 359–363 (2016).
[16] G. Vampa, T. J. Hammond, N. Thiré, B. E. Schmidt, F. Légaré, C. R. McDonald, T. Brabec, and P. B. Corkum, Nature **522**, 462–464 (2015).
[17] M. Hohenleutner, F. Langer, O. Schubert, M. Knorr, U. Huttner, S. W. Koch, M. Kira, and R. Huber, Nature **523**, 572–575 (2015).
[18] G. Ndabashimiye, S. Ghimire, M. Wu, D. A. Browne, K. J. Schafer, M. B. Gaarde, and D. A. Reis, Nature **534**, 520–523 (2016).
[19] F. Lu, P. Xia, Y. Matsumoto, T. Kanai, N. Ishii, and J. Itatani, Opt. Lett. **43**, 2720–2723 (2018).
[20] N. J. Jeon, J. H. Noh, Y. C. Kim, W. S. Yang, S. Ryu, and S. I. Seok, Nat. Mater. **13**, 897–903 (2014).
[21] The peaks of the 7th harmonic order of $MAPbBr_3$ energetically overlap with the bandgap located at 2.3 eV, and the 9th harmonic order of $MAPbCl_3$ overlaps with the bandgap at 3.2 eV. Thus, the harmonics spectra may contain a tail on the lower energy side due to photoluminescence and a distortion due to partial reabsorption of the generated harmonics. In addition, the distortion for the other peaks in the harmonic spectra of $MAPbBr_3$ and $MAPbCl_3$ may come from scattering of harmonics because of surface roughness and then even a small misalignment could lead to the observed spectral distortions.
[22] T. Yamada, T. Aharen, and Y. Kanemitsu, Phys. Rev. Lett. **120**, 057404 (2018).
[23] A. Segura, J. Bouvier, M. V. Andres, F. J. Manjon, and V. Munoz, Phys. Rev. B **56**, 4075–4084 (1997).
[24] K. Kaneshima, Y. Shinohara, K. Takeuchi, N. Ishii, K. Imasaka, T. Kaji, S. Ashihara, K. L. Ishikawa, and J. Itatani, Phys. Rev. Lett. **120**, 243903 (2018).
[25] The basic theoretical framework is the same as the one used in Ref. 24.
[26] M. Lindberg and S. Koch, Phys. Rev. B **38**, 3342–3350 (1988).
[27] G. Murtaza and I. Ahmad, Physica B **406**, 3222–3229 (2011).
[28] W.-J. Yin, J.-H. Yang, J. Kang, Y. Yan, and S.-H. Wei, J. Mater. Chem. A **3**, 8926–8942 (2015).